The Role of Stratospheric Polar Vortex Breakdown in Southern Hemisphere Climate Trends

LANTAO SUN

National Center for Atmospheric Research, Boulder, Colorado*

GANG CHEN

Department of Earth and Atmospheric Sciences, Cornell University, Ithaca, New York

WALTER A. ROBINSON

Department of Marine, Earth, and Atmospheric Sciences, North Carolina State University, Raleigh, North Carolina

(Manuscript received 16 September 2013, in final form 7 March 2014)

ABSTRACT

This paper investigates the connection between the delay in the final breakdown of the stratospheric polar vortex, the stratospheric final warming (SFW), and Southern Hemisphere climate trends. The authors first analyze Interim European Centre for Medium-Range Weather Forecasts (ECMWF) Re-Analysis (ERA-Interim) and three climate model outputs with different climate forcings. Climate trends appear when there is a delay in the timing of SFWs. When regressed onto the SFW dates (which reflect the anomaly when the SFW is delayed for one standard deviation of its onset dates), the anomaly pattern bears a resemblance to the observed climate trends, for all the model outputs, even without any trends. This suggests that the stratospheric and tropospheric circulations are organized by the timing of SFWs in both the interannual time scale and climate trends because of external forcings.

The authors further explore the role of the SFW using a simplified dynamical model in which the ozone depletion is mimicked by a springtime polar stratospheric cooling. The responses of zonal-mean atmospheric circulation, including zonal wind, temperature, and poleward edge of the Hadley cell and the Ferrel cell, are similar to the observed climate trends. The authors divide the years into those in which the SFW is delayed and those in which it is not. The responses for the years in which the SFW is delayed are very similar to the overall response, while the stratosphere is only characterized by the localized cooling for those years in which the SFW is not delayed, with no subsequent downward influence into the troposphere. This suggests that, in order to affect the troposphere, ozone depletion must first delay the SFW so as to induce a deep response in planetary wave drag and the associated eddy-driven circulation.

1. Introduction

The Southern Hemisphere (SH) polar stratosphere has cooled in the spring and summer in the late twentieth century, mainly because of anthropogenic ozone depletion (e.g., Thompson and Solomon 2002). This cooling trend results in a stronger polar vortex, and it delays the final breakdown of the polar vortex, the stratospheric final warming (SFW), in late spring by about 10 days decade^{-1} (e.g., Waugh et al. 1999; Black and McDaniel 2007b). Current chemistry–climate models successfully simulate the cooling trend and strengthening zonal winds in the high latitudes of the SH stratosphere (e.g., Son et al. 2008). These stratospheric trends can induce significant changes in the SH tropospheric circulation, including the poleward shift of the eddy-driven jet and the poleward expansion of the Hadley circulation (e.g., Thompson and Solomon 2002; Son et al. 2009; Thompson et al. 2011). Although the model simulations have been well documented [see Polvani et al. (2011) and references therein],

*The National Center for Atmospheric Research is sponsored by the National Science Foundation.

Corresponding author address: Lantao Sun, National Center for Atmospheric Research, 1850 Table Mesa Drive, Boulder, CO 80305.
E-mail: lantao@ucar.edu

DOI: 10.1175/JAS-D-13-0290.1

© 2014 American Meteorological Society

a comprehensive understanding of how stratospheric ozone depletion influences the SH tropospheric climate is still lacking.

The final breakdown of the SH stratospheric polar vortex plays a critical role in the high-latitude distribution of ozone and its downward influence on the tropospheric climate. Since the seasonal breakup of the polar vortex fills the Antarctic ozone hole with ozone-rich subpolar air, a delay in the vortex breakup delays the seasonal recovery of polar ozone (Salby and Callaghan 2007). This, in turn, reduces the solar heating that otherwise would weaken the vortex, and it further postpones the final collapse of the polar vortex. In addition, the SH stratosphere is most disturbed in the spring and its downward influence on the troposphere takes place in November and December (Hartmann et al. 2000; Baldwin et al. 2003), when the vortex is being eroded by radiative heating and planetary wave breaking. A delay in the SFW is accompanied by a delay in the zonal wind deceleration (Black and McDaniel 2007b), in the stratospheric wave drag and residual vertical circulation (McLandress et al. 2010), and in the downward wave coupling between the stratosphere and the troposphere (Shaw et al. 2010; Harnik et al. 2011). On interannual time scales, SFW events are observed to influence the seasonal transition of the tropospheric circulation, advancing or delaying it 1 or 2 weeks (Black et al. 2006; Black and McDaniel 2007b). These observational results are supported by idealized model simulations with a prescribed seasonal cycle applied only in the stratosphere (Sun and Robinson 2009; Sun et al. 2011).

The main purpose of this study is to investigate the role of stratospheric vortex breakdown in Southern Hemisphere climate trends. Specifically, we show that the delay of the SFW is necessary for the ozone depletion to influence the tropospheric circulation and that the interannual variability in the stratospheric and tropospheric circulation is organized by the timing of the SFW. The work is further motivated by modeling studies that on interannual time scales, the polar cap temperature at 100 hPa and the tropospheric jet location are not well correlated in the austral summer, when the tropospheric response to ozone depletion is strongest (Polvani et al. 2011). We show that this counterintuitive result can be explained, at least partly, by considering the interannual variability of SFW onset dates.

The Interim European Centre for Medium-Range Weather Forecasts (ECMWF) Re-Analysis (ERA-Interim) and three climate model outputs with different climate forcings are used for the trend and regression analysis to elucidate the role of the SFW onset date in causing stratospheric and tropospheric changes. We also run two sets of experiments in a simplified dynamical model, with and without a polar stratospheric cooling in the springtime, to mimic the Antarctic "ozone hole." We compare the circulation response for those years in which the SFW is delayed, and those in which it is not, under the same stratospheric forcing. The circulation response, including the shifts of the tropospheric jet and poleward edge of the Hadley cell and the Ferrel cell, is similar to the observed behavior of the Southern Hemisphere only when the SFW is delayed. In years in which the SFW is not delayed, the response to the stratospheric cooling is characterized only by localized cooling, with no subsequent downward influence. This suggests that ozone depletion affects the Southern Hemisphere climate by delaying the SFW.

This paper is organized as follows. In section 2, we use reanalysis and climate models to perform the climate trend and regression analysis. We present the idealized simulations in section 3, comparing the circulation responses between delayed and undelayed SFWs. The results are discussed in section 4, followed by the final summary and conclusions. Some technical details of the idealized model are summarized in the appendixes.

2. Reanalysis and climate model output diagnostics

a. Data description and SFW onset date calculation

We analyze the reanalysis dataset from ERA-Interim (Dee et al. 2011). The global climate model simulations are from two global atmosphere–land models developed at the Geophysical Fluid Dynamics Laboratory (GFDL) Atmospheric Model 2 (AM2) (Anderson et al. 2004) and Atmospheric Model with Transport and Chemistry (AMTRAC) (Austin and Wilson 2006). The AM2 output comprises two 10-member ensembles forced by (i) observed changes in sea surface temperatures (SST), sea ice, and radiative forcings, denoted AM2(SST+RAD), and (ii) observed changes in SSTs and sea ice with fixed preindustrial radiative forcings, denoted AM2(SST only). These simulations have a coarse resolution in the stratosphere, and the variability and trends of ozone concentration are prescribed. AMTRAC, on the other hand, is a chemistry–climate model based on AM2. It has 48 vertical levels from 0.0017 hPa to the ground, with half of the vertical levels in the stratosphere, as compared with the 4 levels in the stratosphere and the top level at 9 hPa in AM2. AMTRAC includes interactive ozone chemistry, in which the changing concentrations of ozone-depleting substances (ODS) are specified. The REF-B1 simulation (Austin and Wilson 2006), forced by observed changes in SSTs, sea ice, and radiative forcings, is analyzed and denoted AMTRAC (SST+RAD).

All trends in the reanalysis and climate models are calculated for each day of the annual cycle after the daily data are smoothed using a Gaussian window with a 7-day half-width. Changing the strength of the smoothing does not change the structures of the trends. Decadal linear trends for ERA-Interim are calculated for the period 1980–2001, while trends are calculated over the period 1960–99 for the simulations to improve their statistical reliability. Because trends are analyzed over different periods in the simulations and the reanalysis, only a qualitative comparison of these trends is possible. We considered using the 40-yr ECMWF Re-Analysis (ERA-40) (Uppala et al. 2005) and including the period 1960–79, but we question the reliability of Southern Hemisphere reanalysis products prior to the satellite era. Specifically, we compare the austral autumn polar cap temperature at 100 hPa in the reanalysis with the radiosonde data from Antarctica (Screen and Simmonds 2012). In the stratosphere, while the reanalysis closely tracks the observations within the satellite era, they diverge in the earlier period, especially before 1975.

The timing of stratospheric final warming can be defined at stratospheric high latitudes using potential vorticity (Waugh et al. 1999; Zhou et al. 2000), zonal-mean zonal wind at the jet core (Black and McDaniel 2007b), or temperature (Haigh and Roscoe 2009). These approaches, which represent various aspects of the breakdown of the SH polar vortex, yield different SFW onset dates. Given suitable parameters, however, the variability in the timing of the breakup is qualitatively the same (Waugh et al. 1999). Haigh and Roscoe (2009) found that the temporal evolution of onset dates derived from observed Antarctic temperatures was consistent with the results of Black and McDaniel (2007b). These studies suggest that the variability of SFW is insensitive to its precise definition. We adopt the method of Black and McDaniel (2007b) and identify the SFW onset date as the first day of the last time that the 5-day-averaged zonal-mean zonal wind at 50 hPa and 60°S drops below 10 m s^{-1} until the fall.

b. SFW onset date analysis

The top panel of Fig. 1 shows the trends of high-latitude zonal wind and temperature (shading), overlaid with the climatological annual cycle (contours, 1980–2001 average) in ERA-Interim. The annual cycle of the zonal wind is characterized by decelerating stratospheric zonal winds from September to January, with the zero wind line descending from 10 hPa in late November to just above 50 hPa in mid-January. The trend shows increasing zonal winds above 100 hPa throughout the spring and summer, and the stratospheric trend extends downward into the troposphere in December–February,

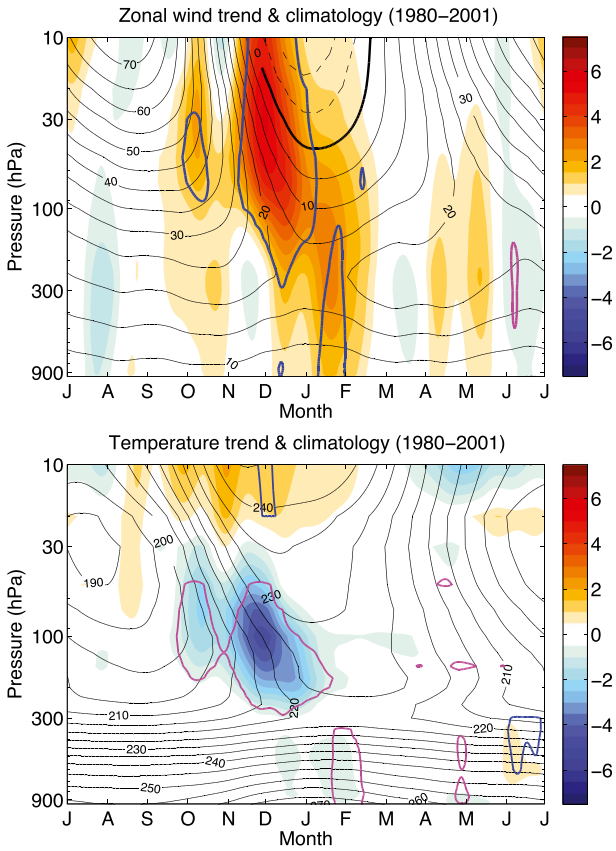

FIG. 1. (top) Zonal-mean zonal wind trend (shading; m s^{-1} decade^{-1}) and climatology (black contour; m s^{-1}) averaged over latitudes 50°–70°S during 1980–2001 in ERA-Interim. (bottom) As in (top), but for polar cap temperature trend (averaged over 60°–90°S; K decade^{-1}) and its climatology (K). Climatology and linear trend are calculated over 1980–2001 for each day of the annual cycle and smoothed by a Gaussian function with a 7-day half-width. Blue and purple lines denote the Student's *t*-test positive and negative 95% statistical significance, respectively. Tick marks on the horizontal axis indicate the first day of the month.

particularly in January. This is consistent with the results obtained by Thompson and Solomon (2002) that Antarctic trends in stratospheric geopotential height lead tropospheric trends by 1–2 months. The annual temperature cycle shows warming of the stratosphere over the same period when the zonal winds are decelerating. There is a cooling trend in temperature between 30 hPa and tropopause that persists from September to January, which is presumably the result of anthropogenic ozone depletion. Overall, the temperature trends are similar to those in Thompson and Solomon (2002) obtained using radiosonde observations.

Trends in stratospheric zonal wind and temperature are strongest in November and December, which implies a delay in the final breakdown of the polar vortex.

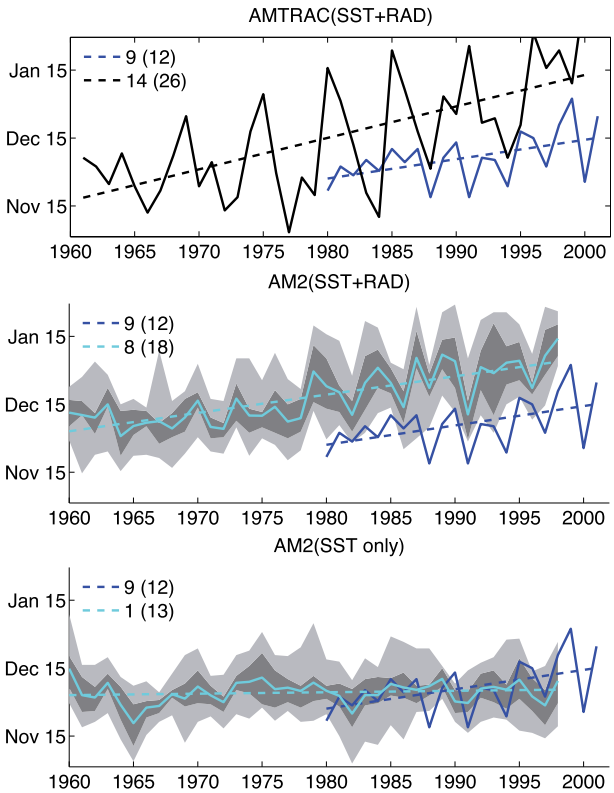

FIG. 2. SFW onset dates at 50 hPa in (top) AMTRAC (SST+RAD), (middle) AM2(SST+RAD), and (bottom) AM2 (SST only). The numbers in the top-left corners denote the linear trend (days decade^{-1}) and standard deviation (number inside the parentheses; days) of the SFW onset dates in models for the period 1960–99, and the blue lines denotes the onset dates in ERA-Interim for the period 1980–2001. The onset dates of 10 realizations in each year in AM2 are ranked in an ascending order as $y_i (i = 1, \ldots, 10)$. The shading is between $(y_1 + y_2)/2$ and $(y_9 + y_{10})/2$, in which the dark shading is between $(y_3 + y_4)/2$ and $(y_7 + y_8)/2$.

Figure 2 shows the SFW onset dates at 50 hPa from 1960 to 1999 in the model simulations along with those in the ERA-Interim dataset (blue line). Table 1 lists the means, standard deviations, and trends of the SFW onset dates for the reanalysis and models. The model forced by an increase in ozone-depleting substances, AMTRAC(SST+RAD), simulates a delay in the SFW of about 14 days decade^{-1}, while in the model forced by the prescribed observed ozone loss, AM2(SST+RAD), the delay is about 8 days decade^{-1}. These values are consistent with the observed delay in the SFW, approximately 9 days decade^{-1} in ERA-Interim over the period 1980–2001. It is noteworthy that the greenhouse gas increase during the same period can also cool the stratosphere, but its effect on the polar vortex breakdown can be ignored, as suggested by the model studies with the ozone change alone (e.g., McLandress et al. 2010). In contrast, the model forced only by observed changed in SSTs, AM2(SST only), has almost no trend in the SFW date. Shaw et al. (2011) investigated the impact of stratospheric ozone depletion on downward wave coupling using models with and without ozone depletion and found that the simulations without ozone depletion do not show a pronounced trend in the date of vortex breakup, with subsequent consequences for stratosphere–troposphere wave coupling. Our finding is consistent with theirs and confirms the importance of ozone depletion in the SFW trend. Note that the delay of the onset dates is insensitive to the latitude and threshold chosen to defined the SFW (not shown).

The SFW onset dates obtained from model runs with observed radiative forcings are approximately 2 weeks later than the observed values for the period 1980–99. This is a common bias among the models participating in the Chemistry–Climate Model Validation (CCMVal) activity (e.g., Austin and Wilson 2010), and phase 5 of the Coupled Model Intercomparison Project (CMIP5) (Wilcox and Charlton-Perez 2013). It is possibly connected to the unresolved orographic gravity waves (Richter et al. 2010; McLandress et al. 2011) in these models.

c. *Climate trends and regression comparisons*

Figure 3 shows the trends in zonal wind averaged over latitudes 50°–70°S for the reanalysis, AMTRAC (SST+RAD), and AM2(SST+RAD) from September to March. The observed trends are reasonably well simulated by AMTRAC with interactive ozone chemistry. With prescribed ozone in AM2, however, the downward influence on the troposphere is much weaker, which is consistent with the results obtained by Son et al. (2008). Trends are absent from AM2(SST only; not shown). We also regress the zonal wind averaged over 50°–70°S on each day of the annual cycle each year $[u(p, d, y)]$ onto the detrended and standardized SFW onset date time series of the corresponding year $[\mathrm{SFW}(y)]$ for the reanalysis and climate models:

$$u(p, d, y) = u_{\mathrm{reg}}(p, d) \times \mathrm{SFW}(y) + \epsilon(p, d, y), \qquad (1)$$

where p denotes the pressure level, y denotes the year of interest, d denotes the day of the annual cycle in year y, and ϵ denotes the pattern unrelated to the SFW variability. Figure 4 shows the regression patterns $u_{\mathrm{reg}}(p, d)$ for the reanalysis and models. The regression pattern reflects the zonal wind anomalies on interannual time scales when the SFW is delayed for one standard deviation of its onset date. A similar pattern can be obtained by taking the difference of the composites for the years with early SFW dates and for the years with late SFW dates. Although the SFW itself represents

TABLE 1. The means, standard deviations, and decadal trends of the SFW onset dates for ERA-Interim, and the simulations of AMTRAC(SST+RAD), AM2(SST+RAD), and AM2(SST only). They are calculated over the period 1980–2001 in the reanalysis and over the period 1960–99 in the AMTRAC and AM2 simulations. The trends of SFW onset dates for the reanalysis, AMTRAC (SST+RAD), and AM2(SST+RAD) are statistically significant at the 99% level, while the trend for AM2(SST only) is not statistically significant. The definition of SFW onset is adopted from Black and McDaniel (2007b).

Datasets	ERA-Interim	AMTRAC(SST+RAD)	AM2(SST+RAD)	AM2(SST only)
Mean onset date	7 Dec	17 Dec	20 Dec	5 Dec
St dev (days)	12	26	18	13
Trend (days decade^{-1})	9	14	8	1

a weakening of the westerlies, the regression here actually shows stronger westerlies for a later onset date. Results for all three simulations and the reanalysis display a downward extension of the stratospheric positive anomaly to the surface. These regression patterns peak at a higher altitude than the strongest climate trends, reflecting the difference between interannual variability (due to the interannual variability of planetary wave forcing) and climate trends (due to ozone forcing in the lower stratosphere). Besides, the regression patterns do not show a month-long delay in the troposphere, and tropospheric anomalies are also much more persistent. Overall, however, the trends in zonal wind are very similar to the response to a delayed SFW within the intrinsic interannual variability of the atmosphere in the reanalysis or the models.

3. Idealized dynamical model simulations

Comprehensive climate models provide credible simulations of the trends and interannual variability in the observations. Because of the complexity of the processes these models represent—dynamics, chemistry, and moist processes, together with multiple external forcings (ODS, greenhouse gases, SST, and sea ice)—it is difficult to attribute the trends captured by these

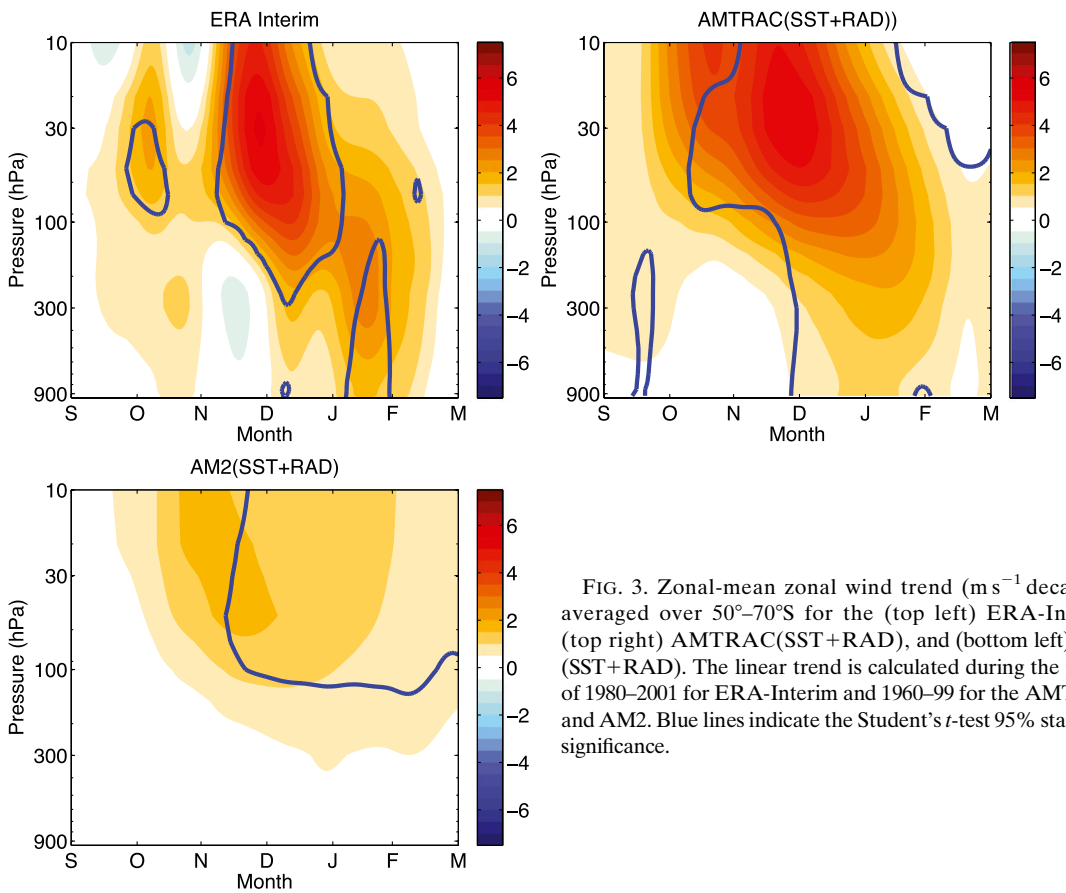

FIG. 3. Zonal-mean zonal wind trend (m s^{-1} decade^{-1}) averaged over 50°–70°S for the (top left) ERA-Interim, (top right) AMTRAC(SST+RAD), and (bottom left) AM2 (SST+RAD). The linear trend is calculated during the period of 1980–2001 for ERA-Interim and 1960–99 for the AMTRAC and AM2. Blue lines indicate the Student's *t*-test 95% statistical significance.

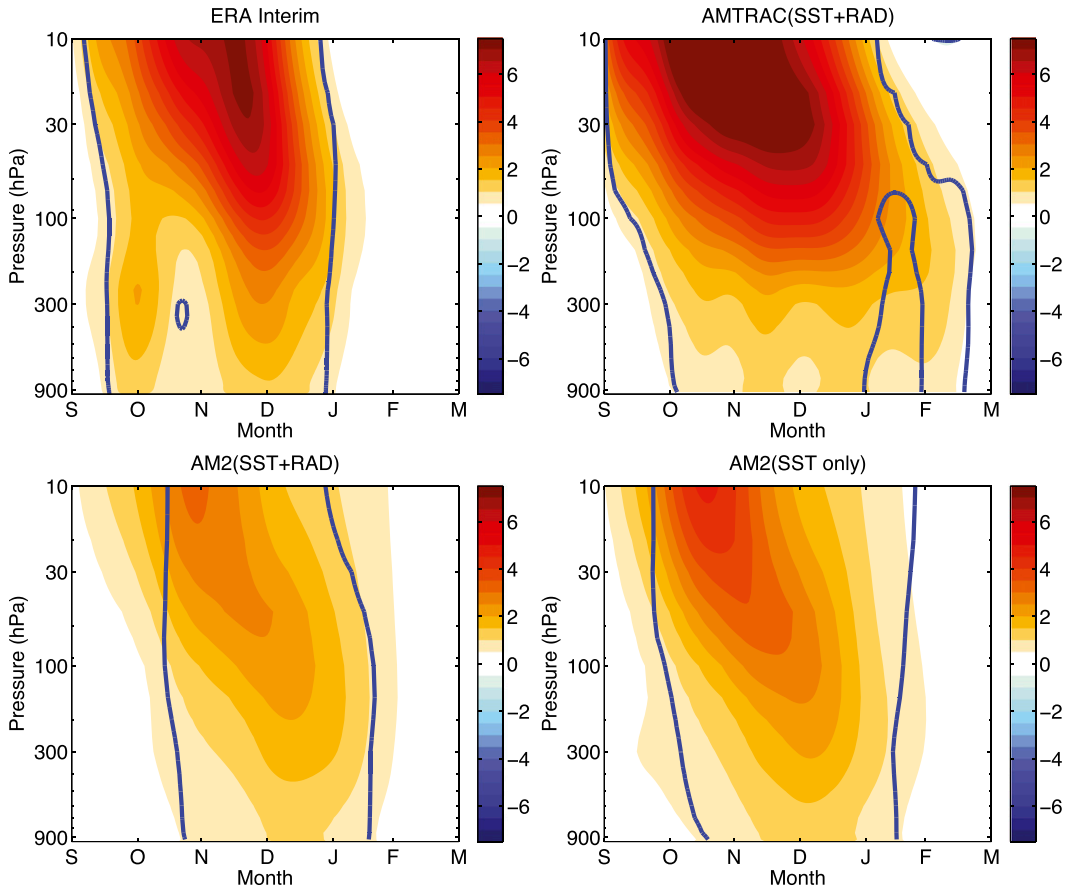

FIG. 4. As in Fig. 3, but for the zonal wind ($\mathrm{m\,s^{-1}}$) regressed onto the detrended SFW onset dates. The regression pattern reflects the zonal wind anomalies on interannual time scales when the SFW is delayed for one standard deviation of its onset date. (bottom right) The result for the AM2(SST only) is included. Blue lines indicate the Student's t-test 95% statistical significance.

models to specific sources. A simplified dry dynamical model, in contrast, can be used to isolate dynamical processes and is suitable for examining the tropospheric response to stratospheric changes.

a. Model description and perturbation

We use the GFDL atmospheric dynamical core with T42 resolution on 40 unevenly spaced sigma levels [as in Chen and Zurita-Gator (2008)]. The model is forced by a relaxation toward a prescribed time-dependent zonally symmetric radiative equilibrium temperature profile and damped by linear drag in the planetary boundary layer. There is no topography. Following Kushner and Polvani (2006), in the stratosphere, we use $\gamma = 6\,\mathrm{K\,km^{-1}}$ to define a midwinter strong polar vortex and $\gamma = 0\,\mathrm{K\,km^{-1}}$ to define a midsummer state. The sinusoidal variation between winter and summer induces the stratospheric seasonal transition. There is no seasonal transition in the troposphere, so that tropospheric response can be attributed solely to the downward influence of the stratosphere. The equations for model radiative equilibrium temperatures can be found in appendix A.

To mimic the thermodynamic effects of ozone depletion, in the perturbation run, we add diabatic cooling to the polar stratosphere in the springtime distributed as follows:

$$Q(\phi,\sigma,t) = q_o \exp\left\{-\left[\frac{(\phi-\phi_o)^2}{2\sigma_\phi^2} + \frac{(-7000\ln\sigma + 7000\ln\sigma_o)^2}{2\sigma_\sigma^2} + \frac{(t-t_o)^2}{2\sigma_t^2}\right]\right\}, \tag{2}$$

where $\phi_0 = -1.57$, $\sigma_\phi = 0.28$, $\sigma_0 = 4000$, and $\sigma_\sigma = 2000$ define the spatial pattern; t_0 (1 October) and $\sigma_t = 20$ days define the peaking time and persistence; and

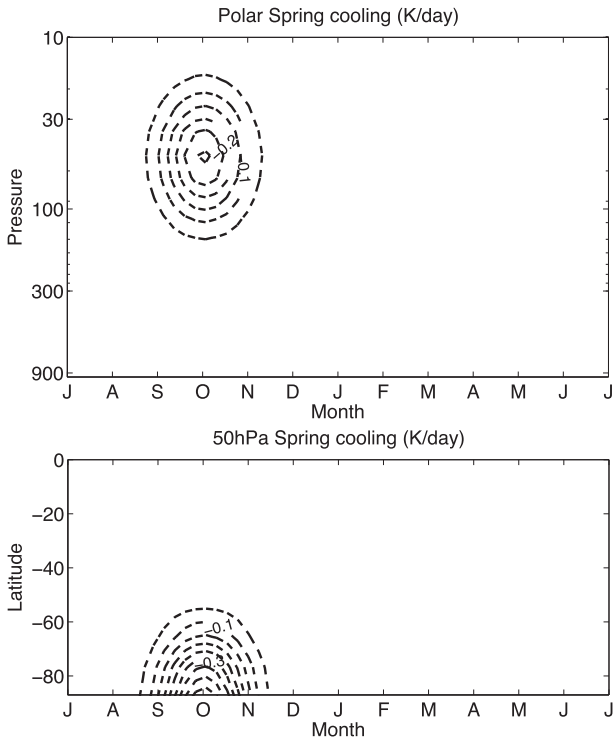

FIG. 5. The vertical and horizontal extents of the polar stratospheric cooling (K day^{-1}) in the dynamical model. (top) Vertical extent over the polar cap (averaged over 60°–90°S). (bottom) Latitudinal cross section at 50 hPa.

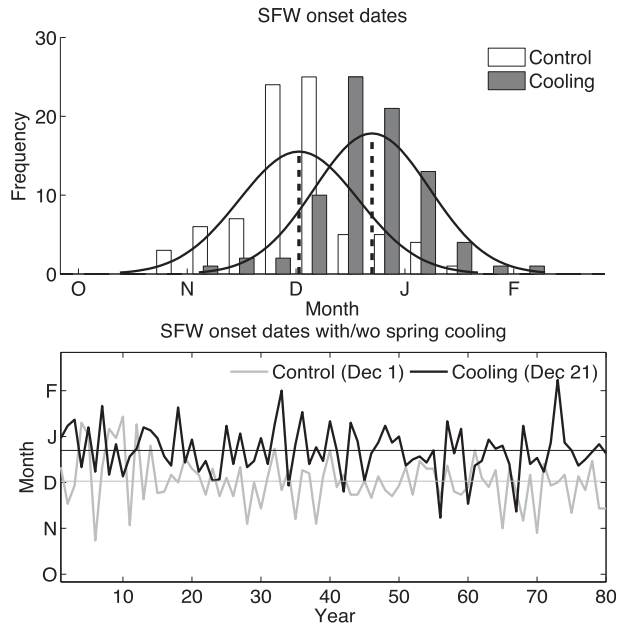

FIG. 6. SFW onset dates at 50 hPa in the control and perturbation runs. (top) Histograms of the onset dates for both experiments and their normal distribution fits. (bottom) 80-yr time series of onset dates. The mean dates for both runs are denoted by thin gray and black lines.

$q_0 = -0.5\,\mathrm{K\,day^{-1}}$. This is analogous to the steady-state polar stratospheric cooling used in Butler et al. (2010) (Table 1; their Figs. 5 and 6). Figure 5 shows the vertical and horizontal extent of this cooling profile and the cooling peaks in October. The profile is similar to the ozone hole evolution used by Polvani et al. (2011) (see their Fig. 1).

We first perform a control run with the seasonal transition only in the stratosphere for 81 years. The last 80 years are branched out and rerun from the stratospheric fall equinox (15 March) for one more year and the extra cooling described by Eq. (2) is applied. In this way, we have 80 realizations of corresponding control and perturbed seasonal simulations. The ensemble-mean anomaly and statistical significance using a Student's t test can be calculated by assuming each year is an independent sample. Given that the observed Southern Hemisphere tropospheric response peaks in austral summer, we add the stratospheric cooling only in the hemisphere with a perpetual summer state in the troposphere (see appendix A for details on the hemisphere asymmetry in the troposphere). Our results remain qualitatively similar even if the tropospheric state is changed to perpetual winter.

In addition to the full model simulations, we use a zonally symmetric model to examine the atmospheric response to this ozone depletion–like polar stratospheric cooling in the absence of eddy feedback. The zonally symmetric model is similar to the full model but only the zonal-mean component (wavenumber 0) is integrated forward in time. The contributions from eddies to the zonal-mean climatology are computed from the daily output of the full model and added as external forcings to the equations of the zonally symmetric model, so that its climatological circulation is the same as in the full model. The same eddy forcing is added to the control run, as well as to the perturbation run with spring cooling. The details of the eddy-forcing calculation are described in the appendix B.

b. *Atmospheric circulation responses*

The probability distributions and time series of SFW onset dates at 50 hPa in the control and perturbation experiments are shown in Fig. 6. The onset date series in the control and perturbation runs indicate interannual variability (bottom panel) and they are approximately normally distributed (top panel). The mean onset date in the control run is 1 December, similar to the observations (7 December). The applied springtime polar stratospheric cooling delays the mean onset date by 20 days. Note that not all final warmings are delayed when the

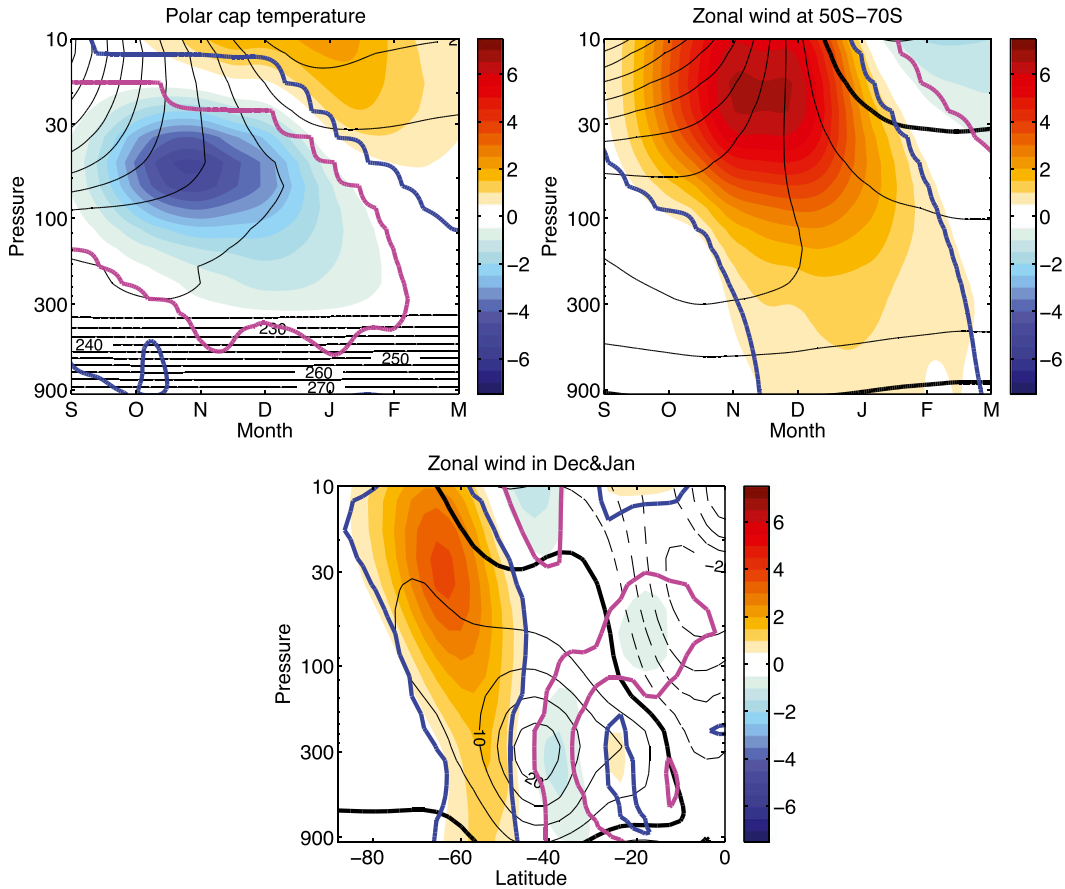

FIG. 7. (top) Zonal-mean anomalies (shading) and climatology (black contour) of (left) polar cap temperature (averaged over 60°–90°S) and (right) high-latitude zonal wind (averaged over 50°–70°S) in the perturbation run. (bottom) Latitudinal cross section of zonal wind anomaly (shading) and its climatology (black contour) averaged over December and January. The blue and purple lines indicate the Student's *t*-test positive and negative 95% statistical significance, respectively.

spring cooling is added to the polar stratosphere: in 14 years, the SFW is earlier in the spring cooling case than in the control and in 1 year, SFW onset date does not change.

The temperature and zonal wind anomalies associated with the polar stratospheric cooling are shown in Fig. 7. Similar to the SH observations shown in Fig. 1, a statistically significant negative temperature anomaly appears in the stratosphere in September, peaking in November, and persisting until February. The polar vortex strengthens and extends downward into the lower troposphere, peaking in December and January. The December–January-mean zonal wind response is shown in the bottom panel of Fig. 7. This zonal wind anomaly is closely aligned with the positive phase of the annular mode simulated by the model; this is also similar to the observations [e.g., Fig. 3 of Chen and Held (2007)].

As the polar vortex strengthens because of ozone depletion, planetary wave propagation changes in the extratropical stratosphere. McLandress et al. (2010) found a weakening of the wave drag prior to early November and strengthening in summer. The top panel of Fig. 8 shows the response of the Eliassen–Palm divergence to springtime polar cooling in our simplified dynamical model. The pattern is similar to that found by McLandress et al. (2010), consistent with their interpretation that the sign reversal between spring and summer is a consequence of the delayed breakdown of SH polar vortex.

The middle panel of Fig. 8 shows the 500-hPa meridional streamfunction response to springtime polar stratospheric cooling and the bottom panel of Fig. 8 shows the December–January mean. In December and January when the tropospheric zonal wind response is strongest, there is a negative response in the streamfunction near the poleward limit of the Hadley cell, which can be defined as the zero streamfunction line near 30°S (thick black line). This indicates a poleward expansion of the Hadley cell. In higher latitudes, a poleward shift of the

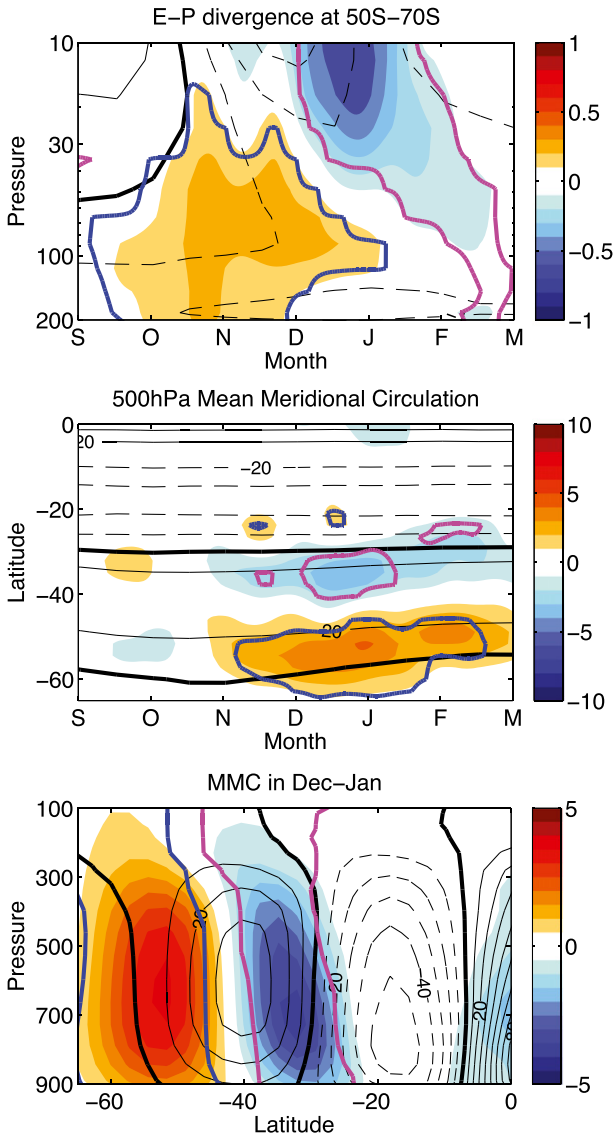

FIG. 8. (top) Eliassen–Palm divergence anomaly (shading) and climatology (black contour, 0.5 m s^{-1} day^{-1}) averaged over 50°–70°S in the perturbation run. (middle) As in (top), but for the 500-hPa MMC anomaly (10^9 kg s^{-1}). (bottom) Latitudinal cross section of MMC anomaly (shading; 10^9 kg s^{-1}) and its climatology (black contour) averaged over December and January. The blue and purple lines indicate the Student's *t*-test positive and negative 95% statistical significance, respectively.

poleward edge of the Ferrel cell, which can be defined as the zero streamfunction near 60°S (thick black line), is also evident. This December–January-mean streamfunction response resembles the pattern found in climate models with stratospheric ozone depletion (e.g., Polvani et al. 2011).

To determine the role of eddies in the atmospheric response to ozone depletion–like polar stratospheric cooling, we apply the same polar stratospheric cooling to the zonally symmetric model, in which the eddy forcing is fixed. Figure 9 (top) shows the temperature and zonal wind anomalies in the zonally symmetric model. Without eddy feedback, the polar vortex strengthens in response to the spring cooling but gradually weakens thereafter. Unlike the full model, the zonal wind anomalies are confined to the stratosphere and there is no downward influence on the troposphere. These differences in responses of the full model and zonally symmetric model indicate that changes in eddy fluxes are necessary to produce the observed impact of ozone depletion on the tropospheric circulation. This is also consistent with the results of the steady-state experiment of Kushner and Polvani (2004), in which they found that the stratospheric thermal perturbation in the absence of eddy feedbacks induced a response that was confined to the stratosphere.

In summary, in a simplified dynamical model, by adding an extra polar stratospheric cooling in the springtime, we find that the polar vortex strengthens and SFWs occur later. The response in extratropical wave drag reverses sign between the spring and summer. In the troposphere, the jet shifts poleward. The Hadley cell expands poleward, as does the Ferrel cell. These responses bear a strong resemblance to the observed and modeled responses to ozone depletion. In the absence of eddy feedback, however, the response is confined to the stratosphere. This highlights the importance of eddies in causing the stratospheric and tropospheric changes.

c. *The role of the SFW in the circulation response*

From Fig. 6, 65 of the 80 SFWs are delayed when the idealized ozone depletion is applied, but there are still 15 cases in which the polar vortex breaks down earlier or on the same day even with the lower-stratospheric cooling. The atmospheric circulation response can be calculated separately for the years in which the SFW is delayed and for those in which it is not in order to elucidate the role of the SFW delay in producing the overall response.

Figure 10 shows the temperature and zonal wind responses for each set of years. For the delayed cases (Fig. 10, right), December temperature decreases and the polar vortex strengthens, which is similar to the total response. In contrast, for the 15 undelayed cases (Fig. 10, left), the polar vortex starts to weaken after mid-November, and the cold anomaly disappears quickly. More importantly, even with the same polar stratospheric cooling in each case, when the SFW is not delayed, there is no significant downward influence into the troposphere.

Figure 11 (top) shows the stratospheric extratropical wave drag responses for delayed and undelayed SFWs. The responses for years with delayed SFWs (Fig. 11, right) are similar to the overall response shown in Fig. 8,

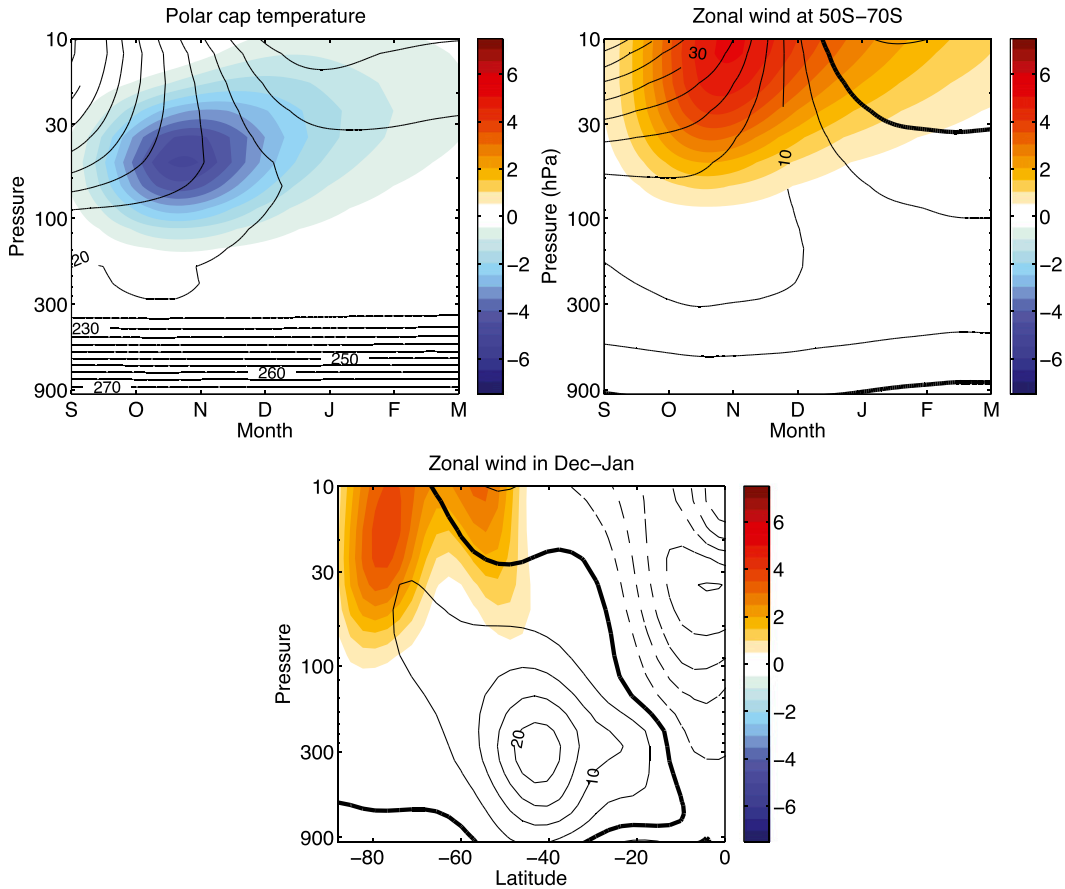

FIG. 9. As in Fig. 7, but for the zonally symmetric model results. In the zonally symmetric model, the same eddy forcings are implied to the control run as well as the perturbation run. See section 3 and appendix B for details.

again. It can be understood from the dynamics of the SFW. From the observations (Black and McDaniel 2007a) and idealized simulations (Sun and Robinson 2009; Sun et al. 2011), the SFW onset is accompanied by a strong eruption of planetary wave activity from the troposphere, so that there is a large zonal wind deceleration in the high latitudes close to the time of the SFW. When the SFW is delayed, this anomalous Eliassen–Palm convergence associated with the planetary wave eruption comes late as well. In turn, there is less wave driving throughout the spring. By contrast, when the SFW is not delayed (Fig. 11, left), there is a strong Eliassen–Palm convergence anomaly in November and December in the middle stratosphere, implying enhanced planetary wave breaking, which is consistent with the earlier vortex breakdown.

Figure 11 (bottom) shows the 500-hPa meridional circulation responses for delayed and undelayed SFWs. The years in which the SFW is delayed display a similar pattern to the overall response shown in Fig. 8. The response for years in which the SFW is not delayed is opposite in sign. Most signals, however, are not statistically significant. This might be related to the small sample size since most of the SFWs occur later in response to our idealized ozone depletion.

The focus of this paper is to investigate the role of the SFW in the stratospheric and tropospheric changes, so the mechanism of how the stratospheric signals extends downward into the troposphere is largely outside our scope. Our idealized experiment results, however, provide some hints about the dynamical mechanisms. The stratospheric influence on the troposphere has been studied in the steady-state experiments (e.g., Kushner and Polvani 2004; Song and Robinson 2004). In these experiments, the synoptic eddy feedback is induced by the tropospheric changes due to changes in stratospheric wave drag, which is normally explained by the "downward control" principle. Here in the context of seasonal transition, we see that the different tropospheric response in Hadley cell extent and jet latitude is similarly related to the wave drag changes in the stratosphere. Specifically, when the SFW is delayed, there is less wave driving in November. Later in December and January, the poleward expansion of the Hadley cell and poleward

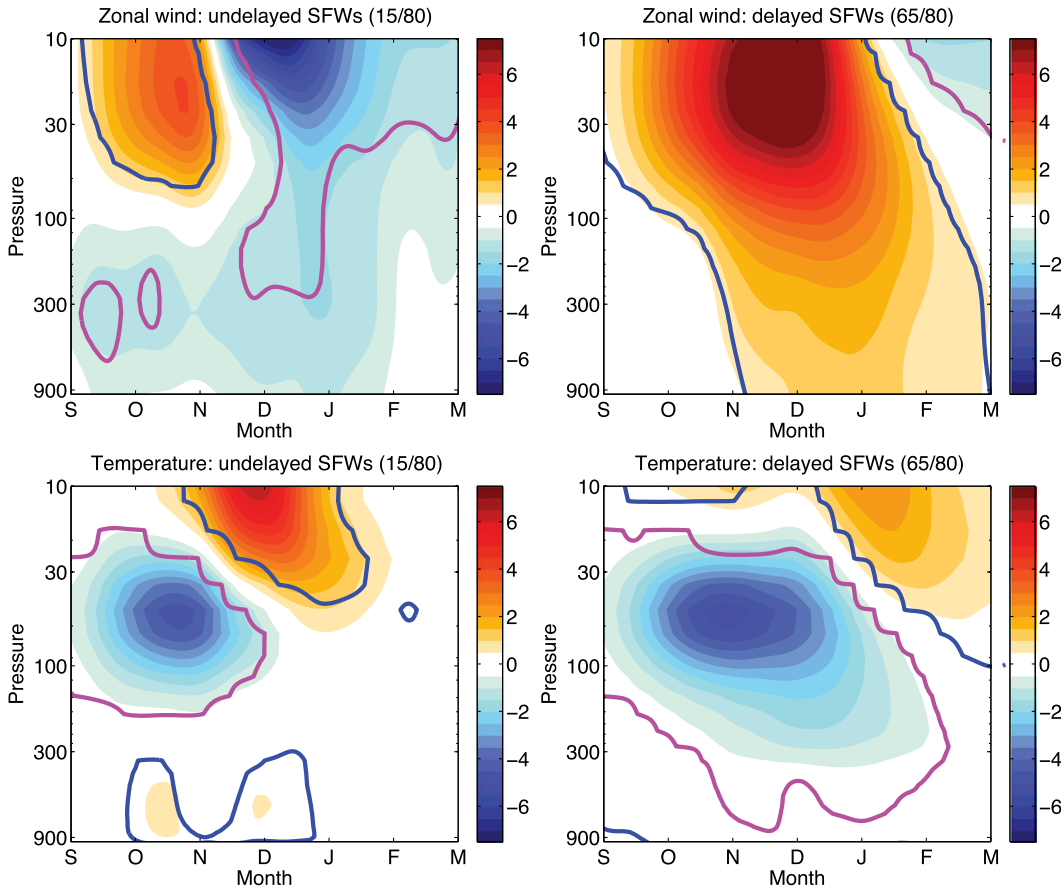

FIG. 10. As in Fig. 7, but only for the years in which (left) the SFW is not delayed in the perturbation run relative to the control run and (right) the SFW is delayed. The blue and purple lines indicate the Student's *t*-test positive and negative 95% statistical significance, respectively.

shift of the tropospheric jet is associated with the changes in stratospheric wave driving. It is important to note that the stronger wave driving in the undelayed case in November and December is much shallower than the weaker wave drag in the delayed case. As a result, despite the enhanced wave drag in the middle stratosphere, the undelayed SFWs do not lead to a noticeable tropospheric signal.

To summarize, the comparison in Figs. 10 and 11 suggests that ozone depletion does not affect the tropospheric circulation in every year. The tropospheric response, including the poleward shift of the jet, poleward expansion of the Hadley cell, and poleward shift of the Ferrel cell are obtained only when there is a delay in the breakdown of the polar vortex.

d. Interannual variability

We can use the control run to investigate the role of the timing of the SFW in causing interannual variability in the stratosphere and troposphere. Similar to Fig. 4, we calculate the regression onto the SFW onset dates for zonal wind, temperature, stratospheric wave drag, and tropospheric mean meridional circulation. These regressions reflect the interannual variability in planetary wave breaking in the stratosphere and the associated responses in the tropospheric circulation.

The top panels of Fig. 12 shows the zonal wind and temperature anomalies when the SFW dates are delayed by one standard deviation. The negative temperature anomalies in the polar stratosphere, strengthening of the polar vortex, and its downward influence closely resemble the climate trends shown in Fig. 7. Figure 12 (bottom) shows the regression for the December–January zonal wind. The positive-annular-mode pattern is very similar to the December–January climate trend. There are differences in stratospheric signals. Ozone depletion occurs in the lower stratosphere, while the planetary wave forcing normally extends downward from the upper stratosphere. Thus, the peak altitude in the climate trends is lower than for the anomalies associated with interannual variability of the SFW dates. A similar difference between internal variability and the response to

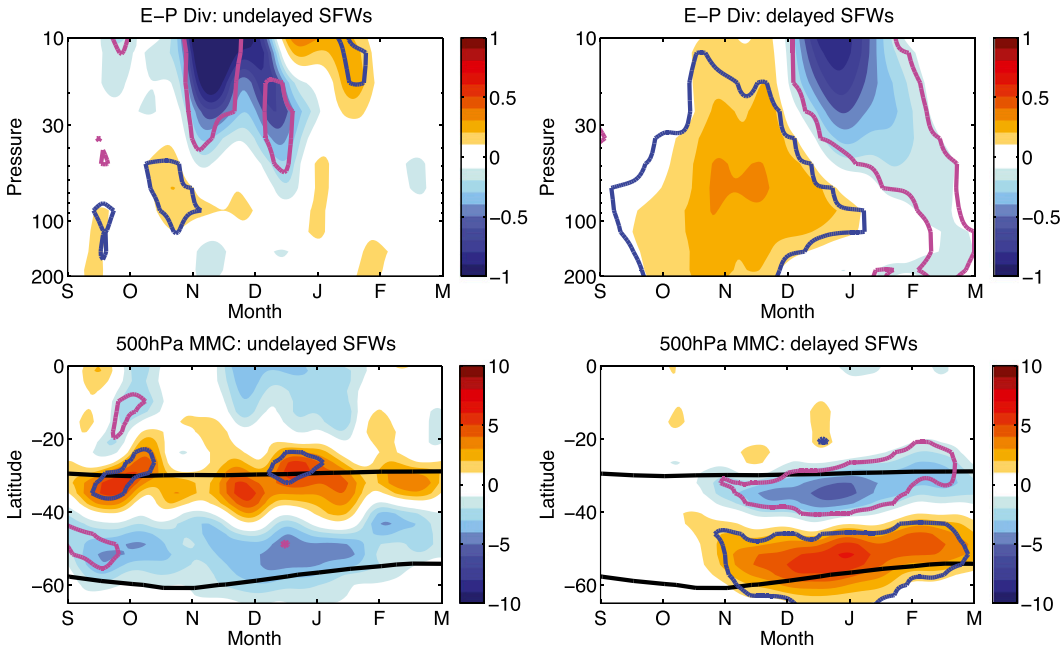

FIG. 11. As in Fig. 8, but only for the years in which (left) the SFW is not delayed in the perturbation run relative to the control run and (right) the SFW is delayed. The thick black lines in the bottom panels denote the edge of the Hadley cell (the lines close to 30°S) and the Ferrel cell (the lines close to 60°S). The blue and purple lines indicate the Student's *t*-test positive and negative 95% statistical significance, respectively.

ozone depletion is found in the climate models and observations (see Figs. 3 and 4).

Figure 13 shows the stratospheric wave drag and tropospheric meridional circulation anomalies associated with delayed SFWs. Consistent with the changes in zonal winds, less planetary wave breaking is found prior to December and more afterward. When the SFW occurs earlier than its climatological date, the pattern of E–P anomalies is the same as that shown in Fig. 13, but with opposite sign. Referring to Fig. 11, increased planetary wave breaking occurs when the SFW is undelayed in the perturbation run, and this is nearly opposite of the pattern shown in Fig. 13. In other words, the E–P anomaly pattern for undelayed SFWs in the perturbation run is very similar to the E–P anomaly pattern for early SFWs in the control run. This points to the role of internal variability in planetary wave driving in producing undelayed SFWs in the perturbation run. The Hadley cell expands poleward and the Ferrel cell shifts poleward as the SFW is delayed (Fig. 13, middle and bottom panels), similar to the climate trends shown in Fig. 11.

4. Discussion

a. Correlation analysis

Polvani et al. (2011) revealed that although there is roughly a linear relationship between the lower-stratospheric temperature trends and the trends in the latitudinal location of the midlatitude jet, the polar cap temperature and the jet location do not appear to be well correlated on interannual time scales. Here we look further into this by calculating their correlation for both the control and perturbation experiments and their separate correlations with the timing of the SFW in our idealized model.

The top panel of Fig. 14 is a scatterplot of polar cap temperature (averaged over 60–90°S) at 100 hPa in December and 850-hPa jet latitude for the period of December–January. Each point indicates one year, and the two big dots indicate the mean of the control and perturbation ensembles. Note from the top-left panel of Fig. 12, the polar cap temperature anomaly at 100 hPa associated with the delay of the SFW is limited to December, so we use the polar cap temperature from this month. From Fig. 14, when the idealized ozone depletion is added in the springtime, there is an ensemble-mean temperature cooling in the polar cap, and zonal winds increase in the high latitudes, indicating a poleward shift of the jet. In terms of the interannual change, however, each point is spread out sporadically and these quantities have a weak correlation (0.37), which is similar to the results shown in Fig. 6a in Polvani et al. (2011).

In the middle (bottom) panel of Fig. 14, we calculate the correlation between polar cap temperature (tropospheric jet latitude) and SFW onset dates. The

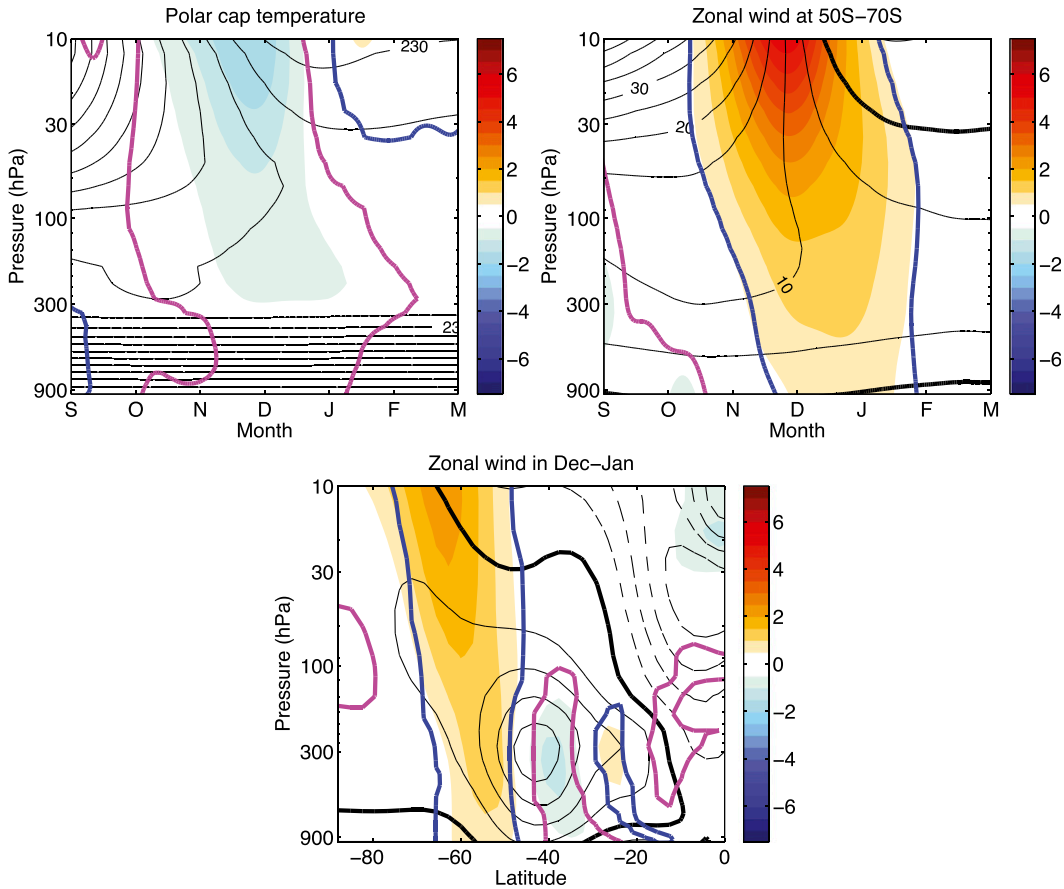

FIG. 12. As in Fig. 7, but for the regression onto the SFW onset dates in the control run. The regression pattern reflects the anomalies on interannual time scales when the SFW is delayed for one standard deviation of its onset date. The blue and purple lines indicate the Student's *t*-test positive and negative 95% statistical significance, respectively.

SFW is delayed and the polar stratosphere is cooled in the ensemble mean when the idealized ozone depletion is applied. More interestingly, the interannual correlation is much stronger (−0.79). The correlation between the timing of the SFW and the tropospheric high-latitude zonal wind (−0.59) is somewhat weaker. This is expected, since the troposphere has intrinsic variability independent of the stratosphere. Nonetheless, the correlations of polar cap temperature and tropospheric zonal wind with the SFW timing are much larger than their own correlation. This suggests that the timing of the polar vortex breakdown is better than polar cap temperature at 100 hPa for characterizing interannual variability of the stratospheric circulation and its downward influence on the troposphere.

We also calculate the correlations separately for the control and perturbation experiments. For all three cases, the correlation for the perturbation experiment is approximately 0.2 larger than for the control experiment. For example, the correlation between the December polar cap temperature at 100 hPa and SFW onset date is −0.57 for the control experiment but −0.82 for the perturbation experiment. This relates to the period over which the average is computed. For SFWs occurring earlier (say, prior to December), the polar cap temperature in November is more sensitive to the timing of the SFW than for a later SFW. Since most SFW onset dates are in December for the perturbation experiments (the average is 20 December), the greater correlation for the perturbation experiment is expected. When the November polar cap temperature is correlated with SFW onset dates, the correlation for the control experiment (−0.78) is stronger than for the perturbation experiment (−0.65).

b. *The connection of the SFW to stratospheric and tropospheric changes*

Figure 15 briefly summarizes the stratospheric and tropospheric changes associated with interannual variability and the forced response to stratospheric cooling by comparing the circulation responses for early and late SFWs in the control run and for delayed and undelayed

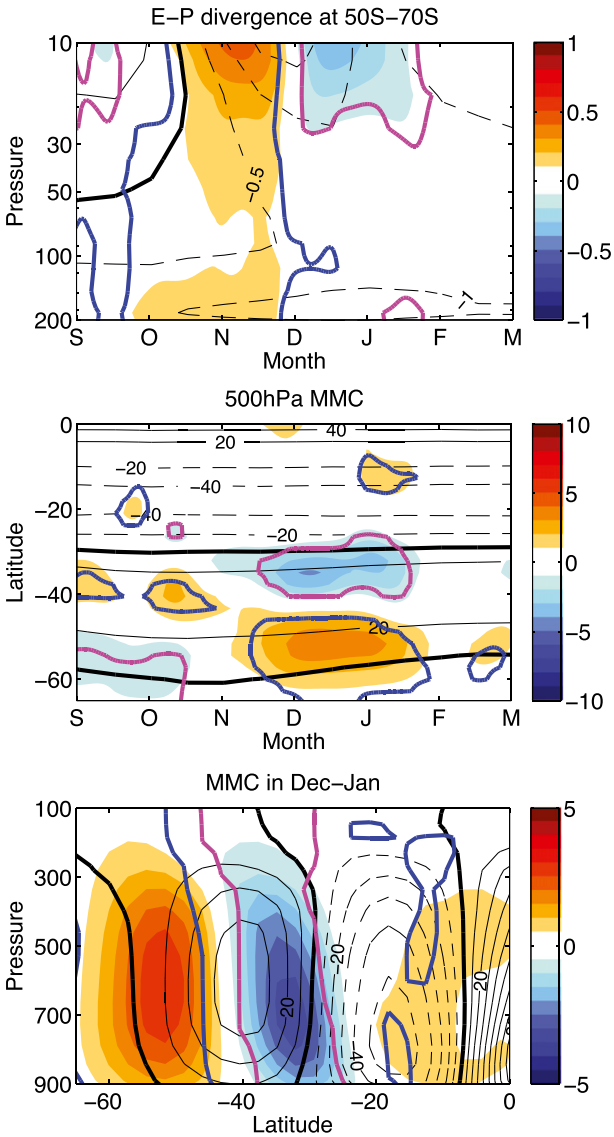

FIG. 13. As in Fig. 8, but for the regression onto the SFW onset dates in the control run. The regression pattern reflects the anomalies on interannual time scales when the SFW is delayed for one standard deviation of its onset date. The blue and purple lines indicate the Student's *t*-test positive and negative 95% statistical significance, respectively.

SFWs between the control run and perturbation run. Figure 15a shows the anomalies for the early and late SFWs, in which the early and late final warmings are defined by deviations of ±0.5 standard deviation from the mean. In accordance with the dynamics of the SFW, the opposite wave drivings in November for the early and late SFWs can be explained by the different timing of the planetary wave eruption (big dots: the mean SFW onset dates). These anomalous strong and weak wave drivings are responsible for the polar cap warming and cooling in the lower stratosphere (second row) and

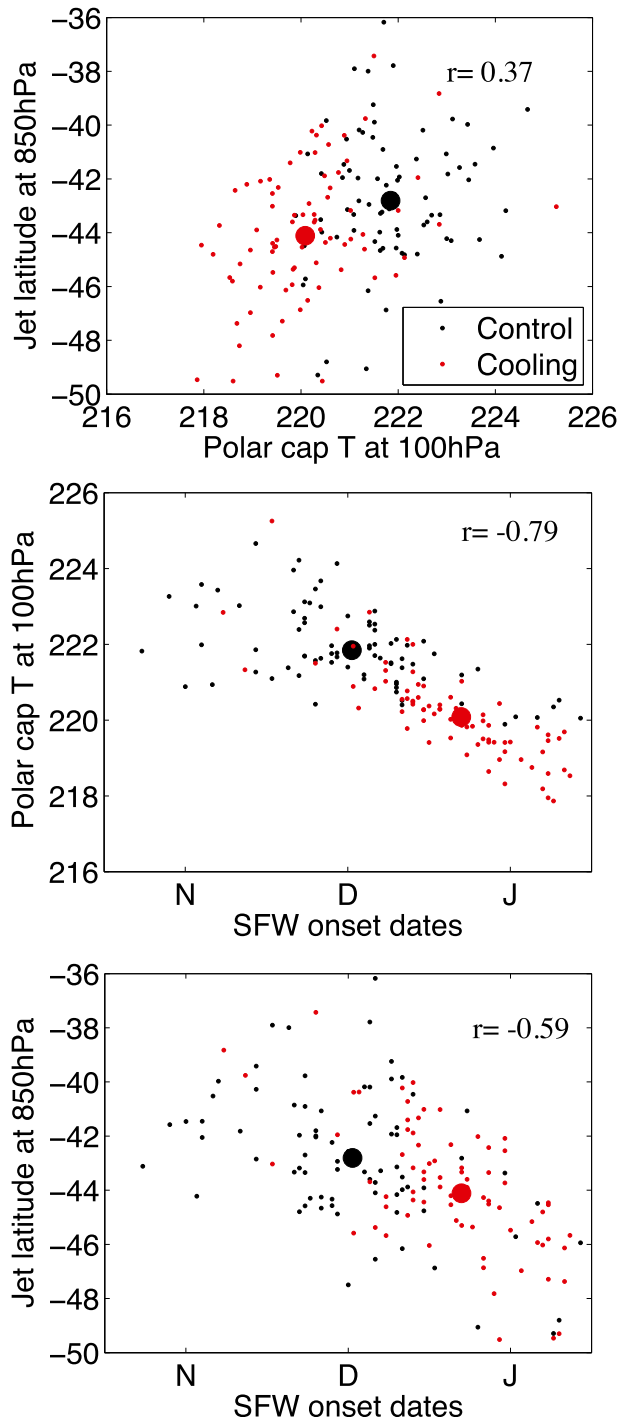

FIG. 14. (top) Scatterplot of polar cap temperature at 100 hPa in December against jet latitude at 850 hPa in December–January. Scatterplots of SFW onset dates at 50 hPa against (middle) polar cap temperature at 100 hPa in December and (bottom) jet latitude at 850 hPa in December–January. Small dots are individual years; large dots are averages over 80-yr realizations. Colors refer to different integrations, as indicated in the legend. The numbers in each plot denote the correlation coefficient, and it is above the 99% statistical significance level for each scatterplot.

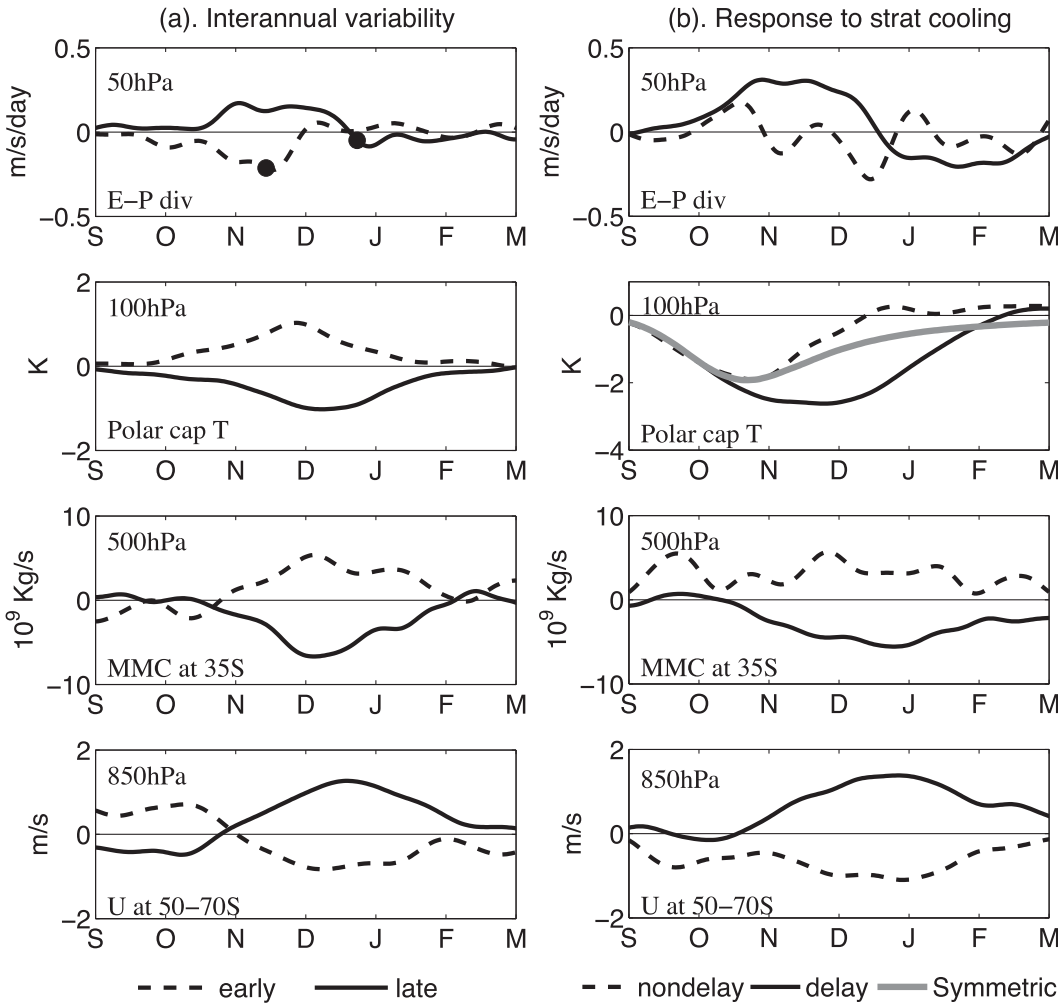

FIG. 15. Stratospheric and tropospheric changes associated with the interannual variability and forced response to the ozone depletion–like polar stratospheric cooling. (a) The anomalies in (first row) 50°–70°S E–P divergence at 50 hPa, (second row) polar cap temperature at 100 hPa, (third row) 35°S MMC at 500 hPa, and (fourth row) 50°–70°S zonal wind at 850 hPa for the years when the SFW occurs early (dashed line) and late (solid line). The large dots denote the early and late SFW onset dates. (b) As in (a), but for years in which the SFW is not delayed (dashed line) and years in which the SFW is delayed (solid line). The polar cap temperature response in the zonally symmetric model is also shown [thick solid gray line in the second row of (b)].

subsequent changes in the troposphere later in December and January (third and fourth rows). In our simulations, the latitude of the Hadley cell edge and the position of the tropospheric jet are highly correlated in December and January [the correlation coefficient is −0.86 between the 850-hPa zonal wind averaged over 50°–70°S and 500-hPa mean meridional circulation (MMC) at 35°S]. This is consistent with the summer results shown in Polvani et al. (2011) in the climate model simulations and suggests that both could be induced by the same synoptic eddies feeding back to the stratospheric changes.

Figure 15b shows the anomalies for the undelayed and delayed SFWs. Interestingly, the circulation responses for the delayed SFWs are very similar to the late SFWs in the control run, including the weak wave driving in the stratosphere in the springtime and tropospheric response later. There are only 15 samples for the undelayed cases, so the signals are noisy. Nevertheless, the reversal in sign in comparison with the delayed SFWs is clear. In addition, much of the temperature anomalies in the lower stratosphere (second row) are due to the polar stratospheric cooling that we applied. For comparison, we also show the polar cap temperature response in the zonally symmetric model. If we subtract the contribution of this ozone depletion–like spring cooling, the temperature anomalies for the undelayed and delayed cases resemble the early and late SFWs in the interannual variability.

Overall, we find that the interannual variability and climate trend of the wave driving in the stratosphere can be largely explained by the changes in the timing of SFWs. Subsequently, these wave drag anomalies are able to trigger the tropospheric eddy feedback—similar to the steady-state experiments shown in Kushner and Polvani (2004) and Song and Robinson (2004). The relative role of different components of the eddies will be discussed in a separate paper (Yang et al. 2014, manuscript submitted to *J. Atmos. Sci.*).

Our results do not contradict the conclusions of Sheshadri et al. (2014), who found that the recent trends in surface westerlies cannot be explained solely by the delay in the timing of final warmings. Black et al. (2006) showed that, in the Northern Hemisphere, the pace of the zonal wind transition is different in early and late final warmings (bottom panel of their Fig. 2). This is also true in the Southern Hemisphere (not shown). Thus, the delay in Antarctic polar vortex breakdown is accompanied by changes in the evolution of stratospheric final warmings. These differences among stratospheric final warmings, together with the delay in vortex breakdown, determine the recent trends in the stratosphere and troposphere. Further quantification of the importance of these two effects in driving surface trends can be obtained by a complex decomposition of the trends, but this is beyond the scope of this paper.

5. Summary and conclusions

In this paper, we use reanalysis, climate model outputs with different climate forcings, and idealized simulations to investigate the role of stratospheric vortex breakdown in producing observed trends in the Southern Hemisphere. Our finding can be summarized as follows.

First, we present the connection among ozone depletion, the timing of SFWs, and the austral climate trends. Observations indicate that ozone depletion causes the polar vortex to strengthen, thereby delaying the SFWs and leading to a subsequent tropospheric response. In AMTRAC(SST+RAD), AM2(SST+RAD), and in a dynamical model with an idealized "ozone depletion," we find similar changes in the circulation in the stratosphere and troposphere. In contrast, in AM2(SST only), without stratospheric forcing, there is no trend in the timing of the SFWs and no discernible trend in tropospheric circulation. When dynamical fields are regressed onto the date of the SFW each year, the anomalies associated with a delayed SFW always show similar patterns to the climate trends associated with ozone depletion. Resemblance between the climate trends and regression anomalies (see Figs. 3 and 4, Figs. 7 and 8, and Figs. 12 and 13) suggests that the stratospheric and tropospheric circulations are organized by the timing of SFWs, not only at the interannual time scale, but also in climate trends owing to external forcings.

Second, in the dynamical model, by dividing years into those in which the SFW is delayed by ozone depletion, and those in which it is not, we expose the critical role of polar vortex breakdown in producing climate trends. In particular, even though the SFW is delayed in most years in response to the springtime polar stratospheric cooling, in some years the SFW occurs earlier. This can be related to interannual variability in the planetary wave breaking. When the SFW is not delayed, the stratospheric and tropospheric responses are distinct from those when the SFW is delayed, and there is no downward influence into the troposphere. In these undelayed years, although the planetary wave drag is enhanced to counteract the zonal wind acceleration, the vertical extent of anomalous wave drag is shallow and has little tropospheric influence. This implies that in order to affect the troposphere, ozone depletion must first delay the SFW so as to generate a deep vertical response in planetary wave drag.

Third, we find that the timing of polar vortex breakdown is better than polar cap temperature at 100 hPa for characterizing stratospheric changes and subsequent tropospheric responses. Previous studies revealed that the interannual variability in polar cap temperature at 100 hPa and tropospheric jet location are only weakly correlated (Polvani et al. 2011). By considering the SFW onset dates, we find that stratospheric polar cap temperature and tropospheric high-latitude zonal wind are better correlated with SFW onset date than with each other. This further highlights the role of the SFW in climate variability and could have implications for the analysis of other datasets (e.g., CMIP5).

Finally, in the context of the winter-to-summer seasonal transition, we find that the summer tropospheric changes in the early (undelayed) and late (delayed) SFWs can be attributed to the differences in stratospheric wave driving in the springtime. These wave driving anomalies can be largely explained by the changes in the timing of SFWs. Specifically, since the polar vortex breakdown coincides with the eruption of planetary wave activity, the early and late occurrences of the SFW will induce stronger or weaker wave driving in the stratosphere, with subsequent tropospheric changes. In the absence of eddy changes in the stratosphere and troposphere, there is no downward influence (Fig. 9).

In conclusion, we find that the spring breakdown of the stratospheric polar vortex plays a crucial role in Southern Hemispheric climate trends and variability. It will, therefore, not be possible to simulate Southern Hemisphere climate trends without first obtaining the

correct trend in the timing of the SFW. The onset date for the SFW is generally too late in the current climate models (e.g., Wilcox and Charlton-Perez 2013), and it is unclear how this affects simulated or projected trends in the Southern Hemisphere climate. Simpson et al. (2011) suggest that this bias could contribute to the too-persistent southern annular mode anomaly, and we speculate that the evolution of the tropospheric response could be different as well.

Acknowledgments. The authors thank Alan Plumb, John Austin, Lorenzo Polvani, Clara Deser, Tiffany Shaw, and David Schneider for valuable discussions and Thomas Delworth for access to GFDL AM2.1 runs. James Screen kindly provided the Antarctic radiosonde data for the comparison with the reanalysis. We are grateful to two anonymous reviewers and Editor Rolando Garcia for comments and suggestions. The ERA-Interim dataset is downloaded from CISL research data archive at NCAR. LS and GC are supported by the National Science Foundation (NSF) climate and large-scale dynamical program under Grant AGS-1042787. LS is also partly supported by the NSF Arctic sciences program.

APPENDIX A

T_{eq} Setup in the Dynamical Model

We use the GFDL atmospheric dynamical core for the idealized model simulations. As in Kushner and Polvani (2006), the model is driven by a relaxation toward a prescribed time-dependent zonally symmetric radiative equilibrium temperature T_{eq} in the stratosphere,

$$T_{eq}^{strat}(\phi,p,t) = [1 - W(\phi,t)]T_{US}(p) + W(\phi,t)T_{PV}(p), \tag{A1}$$

where ϕ is latitude, p is pressure, and $T_{US}(p)$ is the U.S. standard temperature as a function of pressure. The variable $T_{PV}(p)$ is the midwinter polar vortex T_{eq} value,

$$T_{PV}(p) = T_{US}(p_T)(p/p_T)^{R\gamma/g}, \tag{A2}$$

where $p_T = 100$ hPa is a nominal tropopause height, R is the dry air constant, and g is the acceleration of gravity. The lapse rate of $T_{PV}(p)$, $\gamma = 6\,\mathrm{K\,km^{-1}}$, determines the strength of the midwinter polar vortex. The weighting function is

$$W(\phi,t) = \frac{1}{2}(A_S(t)\{1 + \tanh[(\phi - \phi_{0S})/\delta\phi_S]\} + A_N(t)\{1 + \tanh[(\phi - \phi_{0N})/\delta\phi_N]\}), \tag{A3}$$

where $A_S(t) = \max\{0.0, \sin[2\pi(t - t_0)/\Delta T]\}$, $t_0 = 180$ days, $\Delta T = 360$ days, $A_N(t) = \max\{0.0, \sin[2\pi t/\Delta T]\}$, $\phi_{0S} = -50°$, $\phi_S = -10°$, $\phi_{0N} = 50°$, and $\phi_N = 10°$ latitude. The stratospheric equilibrium temperature $T_{eq}^{strat}(\phi, p, t)$ thus varies between midwinter condition ($\gamma = 6\,\mathrm{K\,km^{-1}}$) and midsummer condition ($\gamma = 0\,\mathrm{K\,km^{-1}}$) over a 360-day year.

The tropospheric equilibrium temperature is fixed so that there is no seasonal transition in the troposphere. It is given by

$$T_{eq}^{trop} = \max[T_{US}(p_T), (T_0 - \delta T)(p/p_0)^{\kappa}], \tag{A4}$$

where $T_0 = 315$ K, $p_0 = 1000$ hPa, and $\kappa = 2/7$, with

$$\delta T = \delta_y \sin^2\phi + \epsilon \sin\phi + \delta_z \log(p/p_0)\cos^2\phi, \tag{A5}$$

where $\delta_y = 60$ K, $\delta_z = 10$ K, and $\epsilon = 10$ K. This nonzero value of ϵ provides a simple asymmetry between the perpetual winter (Northern Hemisphere) and perpetual summer hemisphere (Southern Hemisphere).

APPENDIX B

Zonally Symmetric Model

In this paper, we use a zonally symmetric model to simulate the atmospheric response to an ozone depletion–like spring cooling without eddy feedback. In the zonally symmetric model, the initial condition comes from the 80-yr ensemble mean and zonal average of the full model results. The time-evolving eddy forcings are calculated from the full model as well. The method can be illustrated using an advection equation with a damping term

$$\frac{\partial q}{\partial t} = -\mathbf{u}\cdot\nabla q - k(q - q_{eq}) \equiv F(\mathbf{u}, q), \tag{B1}$$

where q is a tracer, k is a damping rate, q_{eq} is a prescribed, time-dependent, and zonally symmetric equilibrium profile of the tracer, and $F(\mathbf{u}, q)$ is an operator for the instantaneous local tendency of q associated with advection and damping. Unlike the Kushner and Polvani (2004) method, we derive the eddy forcing from the instantaneous fields rather than the time-averaged fields. We apply the tendency operator F to the zonal-mean terms

$$\overline{F(\overline{\mathbf{u}}, \overline{q})} = -\overline{\mathbf{u}}\cdot\nabla\overline{q} - k(\overline{q} - q_{eq}) \tag{B2}$$

and then to the total field

$$\overline{F(\mathbf{u}, q)} = -\overline{\mathbf{u}}\cdot\nabla\overline{q} - k(\overline{q} - q_{eq}) - \overline{\mathbf{u}'\cdot\nabla q'}. \tag{B3}$$

Here, the overbars denote the zonal means and primes denote the eddy components. The eddy forcing can be obtained by the difference of the two as

$$\overline{\mathbf{u}' \cdot \nabla q'} = F(\overline{\mathbf{u}}, \overline{q}) - F(\mathbf{u}, q). \tag{B4}$$

The tendency operator is calculated by integrating the primitive equation model forward by one time step using instantaneous daily zonal and meridional winds, temperature, and surface pressure. We first calculate the tendencies for the zonal-mean fields and then compute the tendencies for total field. The difference of the two yields the instantaneous eddy forcing [Eq. (B4)]. Using the primitive-equation model for the tendency calculation ensures that the eddy forcings are consistent with the horizontal and vertical discretization of the numerical model. The daily climatology of the eddy forcing by averaging 80 ensembles is used in the control run as well as the perturbation run with polar stratospheric cooling in the springtime.

REFERENCES

Anderson, J. L., and Coauthors, 2004: The new GFDL global atmosphere and land model AM2–LM2: Evaluation with prescribed SST simulations. *J. Climate,* **17,** 4641–4673, doi:10.1175/JCLI-3223.1.

Austin, J., and R. J. Wilson, 2006: Ensemble simulations of the decline and recovery of stratospheric ozone. *J. Geophys. Res.,* **111,** D16314, doi:10.1029/2005JD006907.

——, and ——, 2010: Sensitivity of polar ozone to sea surface temperatures and halogen amounts. *J. Geophys. Res.,* **115,** D18303, doi:10.1029/2009JD013292.

Baldwin, M. P., D. B. Stephenson, D. W. J. Thompson, T. J. Dunkerton, A. J. Charlton, and A. O'Neill, 2003: Stratospheric memory and skill of extended-range weather forecasts. *Science,* **301,** 636–640, doi:10.1126/science.1087143.

Black, R. X., and B. A. McDaniel, 2007a: The dynamics of Northern Hemisphere stratospheric final warming events. *J. Atmos. Sci.,* **64,** 2932–2946, doi:10.1175/JAS3981.1.

——, and ——, 2007b: Interannual variability in the Southern Hemisphere circulation organized by stratospheric final warming events. *J. Atmos. Sci.,* **64,** 2968–2975, doi:10.1175/JAS3979.1.

——, ——, and W. A. Robinson, 2006: Stratosphere–troposphere coupling during spring onset. *J. Climate,* **19,** 4891–4901, doi:10.1175/JCLI3907.1.

Butler, A. H., D. W. J. Thompson, and R. Heikes, 2010: The steady-state atmospheric circulation response to climate change–like thermal forcings in a simple general circulation model. *J. Climate,* **23,** 3474–3496, doi:10.1175/2010JCLI3228.1.

Chen, G., and I. M. Held, 2007: Phase speed spectra and the recent poleward shift of Southern Hemisphere surface westerlies. *Geophys. Res. Lett.,* **34,** L21805, doi:10.1029/2007GL031200.

——, and P. Zurita-Gator, 2008: The tropospheric jet response to prescribed zonal forcing in an idealized atmospheric model. *J. Atmos. Sci.,* **65,** 2254–2271, doi:10.1175/2007JAS2589.1.

Dee, D. P., and Coauthors, 2011: The ERA-Interim reanalysis: Configuration and performance of the data assimilation system. *Quart. J. Roy. Meteor. Soc.,* **137,** 553–597, doi:10.1002/qj.828.

Haigh, J. D., and H. K. Roscoe, 2009: The final warming date of the Antarctic polar vortex and influences on its interannual variability. *J. Climate,* **22,** 5809–5819, doi:10.1175/2009JCLI2865.1.

Harnik, N., J. Perlwitz, and T. A. Shaw, 2011: Observed decadal changes in downward wave coupling between the stratosphere and troposphere in the Southern Hemisphere. *J. Climate,* **24,** 4558–4569, doi:10.1175/2011JCLI4118.1.

Hartmann, D. L., J. M. Wallace, V. Limpasuvan, D. W. J. Thompson, and J. R. Holton, 2000: Can ozone depletion and global warming interact to produce rapid climate change? *Proc. Natl. Acad. Sci. USA,* **97,** 1412–1417, doi:10.1073/pnas.97.4.1412.

Kushner, P. J., and L. M. Polvani, 2004: Stratosphere–troposphere coupling in a relatively simple AGCM: The role of eddies. *J. Climate,* **17,** 629–639, doi:10.1175/1520-0442(2004)017<0629:SCIARS>2.0.CO;2.

——, and ——, 2006: Stratosphere–troposphere coupling in a relatively simple AGCM: Impact of the seasonal cycle. *J. Climate,* **19,** 5721–5727, doi:10.1175/JCLI4007.1.

McLandress, C., A. I. Jonsson, D. A. Plummer, M. C. Reader, J. F. Scinocca, and T. G. Shepherd, 2010: Separating the dynamical effects of climate change and ozone depletion. Part I: Southern Hemisphere stratosphere. *J. Climate,* **23,** 5002–5020, doi:10.1175/2010JCLI3586.1.

——, T. G. Shepherd, S. Polavarapu, and S. R. Beagley, 2011: Is missing orographic gravity wave drag near 60°S the cause of the stratospheric zonal wind biases in chemistry–climate models? *J. Atmos. Sci.,* **69,** 802–818, doi:10.1175/JAS-D-11-0159.1.

Polvani, L. M., D. W. Waugh, G. J. P. Correa, and S.-W. Son, 2011: Stratospheric ozone depletion: The main driver of twentieth-century atmospheric circulation changes in the Southern Hemisphere. *J. Climate,* **24,** 795–812, doi:10.1175/2010JCLI3772.1.

Richter, J. H., F. Sassi, and R. R. Garcia, 2010: Toward a physically based gravity wave source parameterization in a general circulation model. *J. Atmos. Sci.,* **67,** 136–156, doi:10.1175/2009JAS3112.1.

Salby, M. L., and P. F. Callaghan, 2007: Influence of planetary wave activity on the stratospheric final warming and spring ozone. *J. Geophys. Res.,* **112,** D20111, doi:10.1029/2006JD007536.

Screen, J. A., and I. Simmonds, 2012: Half-century air temperature change above Antarctica: Observed trends and spatial reconstructions. *J. Geophys. Res.,* **117,** D16108, doi:10.1029/2012JD017885.

Shaw, T. A., J. Perlwitz, and N. Harnik, 2010: Downward wave coupling between the stratosphere and troposphere: The importance of meridional wave guiding and comparison with zonal-mean coupling. *J. Climate,* **23,** 6365–6381, doi:10.1175/2010JCLI3804.1.

——, ——, ——, P. A. Newman, and S. Pawson, 2011: The impact of stratospheric ozone changes on downward wave coupling in the Southern Hemisphere. *J. Climate,* **24,** 4210–4229, doi:10.1175/2011JCLI4170.1.

Sheshadri, A., R. A. Plumb, and D. I. V. Domeisen, 2014: Can the delay in Antarctic polar vortex breakup explain recent trends in surface westerlies? *J. Atmos. Sci.,* **71,** 566–573, doi:10.1175/JAS-D-12-0343.1.

Simpson, I. R., P. Hitchcock, T. G. Shepherd, and J. F. Scinocca, 2011: Stratospheric variability and tropospheric annular-mode timescales. *Geophys. Res. Lett.,* **38,** L20806, doi:10.1029/2011GL049304.

Son, S.-W., and Coauthors, 2008: The impact of stratospheric ozone recovery on the Southern Hemisphere westerly jet. *Science,* **320,** 1486–1489, doi:10.1126/science.1155939.

——, and Coauthors, 2009: The impact of stratospheric ozone recovery on tropopause height trends. *J. Climate,* **22,** 429–445, doi:10.1175/2008JCLI2215.1.

Song, Y., and W. A. Robinson, 2004: Dynamical mechanisms for stratospheric influences on the troposphere. *J. Atmos. Sci.,* **61,** 1711–1725, doi:10.1175/1520-0469(2004)061<1711:DMFSIO>2.0.CO;2.

Sun, L., and W. A. Robinson, 2009: Downward influence of stratospheric final warming events in an idealized model. *Geophys. Res. Lett.,* **36,** L03819, doi:10.1029/2008GL036624.

——, ——, and G. Chen, 2011: The role of planetary waves in the downward influence of stratospheric final warming events. *J. Atmos. Sci.,* **68,** 2826–2843, doi:10.1175/JAS-D-11-014.1.

Thompson, D. W. J., and S. Solomon, 2002: Interpretation of recent Southern Hemisphere climate change. *Science,* **296,** 895–899, doi:10.1126/science.1069270.

——, ——, P. J. Kushner, M. H. England, K. M. Grise, and D. J. Karoly, 2011: Signatures of the Antarctic ozone hole in Southern Hemisphere surface climate change. *Nature Geosci.,* **4,** 741–749, doi:10.1038/ngeo1296.

Uppala, S. M., and Coauthors, 2005: The ERA-40 Re-Analysis. *Quart. J. Roy. Meteor. Soc.,* **131,** 2961–3012, doi:10.1256/qj.04.176.

Waugh, D. W., W. J. Randel, S. Pawson, P. A. Newman, and E. R. Nash, 1999: Persistence of the lower stratospheric polar vortices. *J. Geophys. Res.,* **104,** 27 191–27 201, doi:10.1029/1999JD900795.

Wilcox, L. J., and A. J. Charlton-Perez, 2013: Final warming of the Southern Hemisphere polar vortex in high- and low-top CMIP5 models. *J. Geophys. Res.,* **118,** 2535–2546, doi:10.1002/jgrd.50254.

Zhou, S., M. E. Gelman, A. J. Miller, and J. P. McCormack, 2000: An inter-hemisphere comparison of the persistent stratospheric polar vortex. *Geophys. Res. Lett.,* **27,** 1123–1126, doi:10.1029/1999GL011018.